Renewable Energy 165 (2021) 14–27

Contents lists available at ScienceDirect

Renewable Energy

journal homepage: www.elsevier.com/locate/renene

Performance analyses in parabolic trough collectors by inserting novel inclined curved-twisted baffles

Hui Xiao , Peng Liu *, Zhichun Liu , Wei Liu *

School of Energy and Power Engineering, Huazhong University of Science and Technology, Wuhan, 430074, PR China

ARTICLE INFO

Article history:
Received 11 August 2020
Received in revised form
11 November 2020
Accepted 12 November 2020
Available online 17 November 2020

Keywords:
Parabolic trough collector
Curved-twisted baffles
Thermal hydraulic performance
Wall temperature uniformity
Swirls impinging cooling

ABSTRACT

The operation stability demands for low and uniform wall temperature in the parabolic trough collector which acts as an energy conversion component in concentrating thermal conversion technology. In order to reduce the local high temperature with moderate pump power consumption, this paper proposed longitudinal swirls impinging cooling method. Three types of novel inclined curved-twisted baffles (A1, A2, and A3) were devised to realize this method. With selecting the absorber tube as research model, this paper numerically compared the impinging cooling characteristics, wall temperature uniformity performance, and efficiency performance by inserting the three types of baffles. The A1 and A2 types each generated a pair of longitudinal swirls while the A3 type generated two pairs of longitudinal swirls. The impinging cooling always appeared near the front edge of inclined baffles. The A1 type was the best in wall temperature uniformity and efficiencies among three baffles. Furthermore, as the inlet temperature increased from 400 K to 600 K at a mass flow rate of 1.13 kg/s in the A1 type tube, the average wall temperature difference between bottom half tube and top half tube was decreased by 55.1%. Meanwhile, the average overall efficiency and exergy efficiency were increased by 0.52% and 0.22%, respectively.

1. Introduction

Solar energy is a high-grade and abundant renewable energy [1]. The received incident solar irradiation on the earth surface for 84 min would meet the worldwide human energy demand for a year [2]. Concentrating solar power is promising in solar energy utilization [3]. The parabolic trough collector (PTC) is the most mature concentrating solar thermal conversion technologies in temperature levels from 420 K to 770 K at present [4]. PTCs are widely applied in solar refrigeration, desalination, chemical processes, electricity production, and etc. However, the excessive non-uniform high receiver tube temperature deteriorates the operation efficiency and safety [5]. In details, there are three main reasons: (a) the performance of selective coating is usually decreased as the temperature increases; (b) Due to thermal expansion, the bending of receiver tube is increased as the average temperature difference between the bottom half tube wall and the top half tube wall increases; (c) the radiation loss is increased with the increase of wall temperature. Besides, in order to reduce investment, higher concentration ratios and operation temperature would be applied [4]. Therefore, it is of great importance to take heat transfer enhancement measures to decrease and uniform the receiver wall temperature.

Generally, the average wall temperature is decreased as the thermal performance increases. The previous researches related to heat transfer enhancement in the PTC mainly involves nanofluids, new receiver tubes, and inserts [6]. The measure of using nanofluids is aimed at improving the thermal conductivity to enhance the overall heat transfer performance. Subramani et al. [7] experimentally studied the heat transfer enhancement in the PTC using TiO_2/DI-H_2O nanofluid. The enhancement in convective heat transfer coefficient was up to 22.76%. Mwesigye et al. [8] numerically investigated the effect of Cu-TherminolR*R*VP-1 nanofluid on the thermal performance of a high concentration ratio PTC. At the working temperature of 650 K, the thermal efficiency increased up to 12.5% as nanoparticle volume fraction increased up to 6%. Wang et al. [9] numerically investigated the circumferential temperature difference and deformation of the absorber tube using Al_2O_3/synthetic oil nanofluid as heat transfer fluid. It was found that the heat transfer performance was improved, thus avoiding high temperature gradients and diminishing the thermal stress and deformation. Besides, some researchers paid attention to applying new receiver

* Corresponding authors.
E-mail addresses: xiaohui_hust@foxmail.com (H. Xiao), peng_liu@hust.edu.cn (P. Liu), zcliu@hust.edu.cn (Z. Liu), w_liu@hust.edu.cn (W. Liu).

https://doi.org/10.1016/j.renene.2020.11.068
0960-1481/

Nomenclature

A_c	glass cover area
A_r	absorber tube area
c_p	specific heat capacity
D_h	hydraulic diameter
e	baffle height
E_{xd}	exergy destruction
f	friction factor
h	heat transfer coefficient
k	turbulent kinetic energy
l	baffle length
L	test section length
L_{in}	inlet section length
L_{out}	outlet section length
Lu	local heat convection number
m	mass flow rate
Nu	Nusselt number
p	pressure
p_l/D_h	longitudinal pitch ratio
P_w	pump power consumption
Pr	Prandtl number
q	mean wall heat flux
Q_{loss}	heat loss
Q_u	absorbed useful heat
Q_s	irradiation solar energy
Re	Reynolds number
T	temperature
T_a	ambient temperature
T_{btm}	bottom half tube temperature
T_c	glass cover temperature
T_f	bulk fluid temperature
T_{max}	maximum tube temperature
T_{min}	minimum tube temperature
T_r	absorber tube temperature
T_{sky}	sky temperature
T_{tpm}	top half tube temperature
u_m	inlet mean velocity
u,v,w	velocity components
U_L	heat loss coefficient
V_h	heat convection velocity
x,y,z	Cartesian coordinates

Greek symbols

α	inclined angle of baffles
β	synergy angle
ε	energy dissipation rate
ε_c	glass cover emissivity
ε_r	absorber tube emissivity
η_{th}	thermal efficiency
η_{ovr}	overall efficiency
η_{ex}	exergy efficiency
θ	central angle
κ	thermal conductivity
μ	dynamic viscosity
ρ	density
Φ	viscous heat dissipation

tubes to enhancing the thermal performance. Akbarzadeh and Valipour [10] experimentally investigated the effect of helically corrugated tube on the energy and exergy efficiencies in the PTC. The enhancement in exergy and energy efficiencies was observed and the corrugated tube was recommended. Bellos and Tzivanidis [11] proposed a combined measure of internal longitudinal fins and reflecting shield. The thermal efficiency could be enhanced by 0.90%, 1.66%, and 2.41% respectively with only internal fins, only shield, and both fins and shield at the inlet temperature of 650 K. Liu et al. [12] proposed ribbed absorber tube in the PTC. It was numerically found that the heat transfer performance was improved accompanying with maximum reductions in peak temperature and heat loss to 177 K and 80.1%, respectively. New receiver tube demands for more advanced manufacture techniques and tube reliability tests. For the purpose of manufacture convenience and generating more intense fluid disturbance, researchers designed inserts to disturb fluid in the PTC. Jaramillo et al. [13] developed a thermodynamic model framework and predicted the thermal and exergy efficiency of a PTC with inserting twisted tape inserts. They recommended shedding more light in passive heat transfer enhancement techniques such as twisted tape inserts. Mwesigye et al. [14] numerically analyzed the thermal performance in the PTC inserted with centrally placed perforated plates. The receiver temperature gradients was reduced as well as the modified thermal efficiency could increase by 8%. Zhu et al. [15] proposed wavy tape for the PTC and numerically found that the provoked high local heat transfer by the wavy-tape exactly suppressed the high local wall temperature. Liu et al. [16] analyzed the thermal hydraulic performance of a PTC inserted with conical strip inserts. The peak temperature was decreased significantly and the thermal efficiency was increased at low mass flow rate. In general, inserts can mobilize the core flows to boundary region so as to increase the disturbance intensity dramatically near the high temperature wall. Hence, tube inserts are promising heat transfer enhancement components for controlling wall temperature and improving efficiency.

However, the heat transfer enhancement techniques also accompany with dramatically increased flow resistance in the PTC. Some researchers made efforts to find the optimized flow pattern in convective heat transfer process in order to prevent excessive pressure drop. Liu et al. [17] obtained multi-longitudinal swirls flow in circular tube through heat transfer optimization in laminar flow. Xiao et al. [18] obtained multi-longitudinal swirls flow in rectangular duct through heat transfer optimization in turbulent flow. Zheng et al. [19] carried out a comprehensive review on heat transfer techniques which formed longitudinal swirls flow. They found these heat transfer enhancement techniques could achieve excellent heat transfer performance with less pressure drop. In addition, the longitudinal swirls can deflect the cold fluid to impinge the high temperature wall, thereby reducing the local high temperature. Hence, multi-longitudinal swirls flow is a promising flow pattern in the PTC. However, it lacks of relevant heat transfer enhancement components in the PTC.

In this paper, the main focus is to devise effective inserts for forming multi-longitudinal swirls flow in the metallic tube of PTC in order to balance the trade-off between the gains of wall temperature uniformity and the penalty of flow resistance increase. Thus, the three types of inclined curved-twisted baffles are proposed in the receiver tube in this paper. The novelty of this paper contains three points: (a) the longitudinal swirls impinging cooling method (SICM) is proposed for controlling the local high wall temperature in the PTC; (b) novel inclined curved-twisted baffles (ICTB) are proposed to form longitudinal swirls flow in the PTC so as to successfully reduce the wall temperature with moderate power

consumption penalty; (c) the effect of longitudinal swirls flow on the energy and exergy efficiencies are investigated in the PTC with inserting ICTBs.

The following context consists of four parts. The physical models of parabolic trough collector and three types of curved-twisted baffles will be elaborated firstly. Subsequently, the research methods will be introduced. Furthermore, the flow characteristics and wall temperature distributions will be displayed and the performance analyses will be carried out with the variations of mass flow rate and inlet temperature. In the end, typical conclusions will be drawn.

2. Physical model

2.1. Parabolic trough collector

As depicted in Fig. 1(a), the parabolic trough collector consists of a parabolic mirror, a glass cover and a metallic absorber tube. It is nearly vacuum between the metallic tube and glass cover for reducing thermal loss. The parabolic trough collector is similar to the SEGS LS-2 receiver. The detail parameters are taken from the previous works [12,14,20]. The concentration ratio is 86. The rim angle is 80°. The width of the aperture is 6 m. In this paper, the purpose is to enhance the convective heat transfer in the metallic tube. For simplicity, the effect of parabolic trough collector parameters is taken into consideration by imposing non-uniform heat flux on the receiver tube. As for the optical efficiency related to the details of the parabolic trough collector, a value of 0.75 is given. As depicted in Fig. 1(b), the profile of absorber wall heat flux is also adapted from previous works [12,14,20]. Similar heat flux profiles were also seen in other previous works [21–23]. The heat flux imposed on the receiver wall is fairly non-uniform, thereby leading to high local wall temperature. Specially, the average heat flux on the bottom half wall is much larger than that on the top half wall, which causes more thermal strain in the bottom half wall. Consequently, the glass tube may burst due to the tube bending. Thus, it is of significant importance to decrease and uniform the tube wall temperature.

2.2. Present research model

The metallic absorber tube is taken out for investigating the wall temperature distribution and thermal hydraulic performance. As depicted in Fig. 2, the total length is 1.3 m, including inlet section of 0.5 m, test section of 0.6 m, and outlet section of 0.2 m. The tube diameter is 0.066 m, which is similar to the size of common LS2 solar collector [24]. In order to decrease and uniform the wall temperature, the inclined curved-twisted baffles connected with four rods are inserted into the tube. The longitudinal pitch ratio (p_l/D_h) is 1. The details of curved-twisted baffles are displayed in Fig. 3. The baffle height (e) is 0.005 m and the total baffle length (l) is 0.069 m. The inclined angle is 45°. The curved-twisted baffle is obtained through rolling the base plate to arc plate. In practical process, the curved-twisted baffle can be fabricated by 3D print or stamping. In this paper, the performance of three types of curved-twisted baffles will be compared with the increase of mass flux rate from 1.13 kg/s to 10.20 kg/s and inlet temperature from 400 K to 600 K. This operation condition is common in the literatures [25,26].

3. Research methods

3.1. Governing equations

The present problem is three dimensional steady incompressible turbulent flow. The solid domain of the inserts is not considered in this work. The wall surfaces of inserts are still there so that the disturbance caused by inserts is taken into consideration. It is rational to neglect the viscous dissipation, radiation and gravity in the present research. The working fluid is selected as Syltherm 800. Its density, conductivity, and thermal capacity are constant at a given inlet temperature. The viscosity is varied with the variation of local temperature. Thus, the governing equations are expressed as [27]:

Continuity equation:

$$\frac{\partial(\rho u_i)}{\partial x_i} = 0 \tag{1}$$

Momentum equation:

$$\frac{\partial}{\partial x_j}(\rho u_i u_j) = -\frac{\partial p}{\partial x_i} + \frac{\partial}{\partial x_j}\left[\mu_{\text{eff}}\left(\frac{\partial u_i}{\partial x_j} + \frac{\partial u_j}{\partial x_i}\right)\right] \tag{2}$$

Energy equation:

$$\frac{\partial}{\partial x_i}\left(\rho u_i c_p T - \kappa_{\text{eff}}\frac{\partial T}{\partial x_i}\right) = \Phi \tag{3}$$

The realizable k-ε model has been extensively validated for turbulent flows in the parabolic trough collector [12,14,20]. The turbulence model equations are given as [28]:

$$\frac{\partial}{\partial x_i}(\rho k u_i) = \frac{\partial}{\partial x_j}\left(\left(\mu + \frac{\mu_t}{\sigma_k}\right)\frac{\partial k}{\partial x_j}\right) + G_k - \rho\varepsilon \tag{4}$$

$$\frac{\partial}{\partial x_i}(\rho\varepsilon u_i) = \frac{\partial}{\partial x_j}\left(\left(\mu + \frac{\mu_t}{\sigma_\varepsilon}\right)\frac{\partial \varepsilon}{\partial x_j}\right) + \rho C_1 S\varepsilon - \rho C_2\frac{\varepsilon^2}{k + \sqrt{\nu\varepsilon}} \tag{5}$$

where $\mu_{\text{eff}} = \mu + \mu_t$, $\mu_t = \rho C_\mu k^2/\varepsilon$, $\kappa_{\text{eff}} = \kappa + \mu_t/\text{Pr}_t$, $\text{Pr}_t = 0.85$,

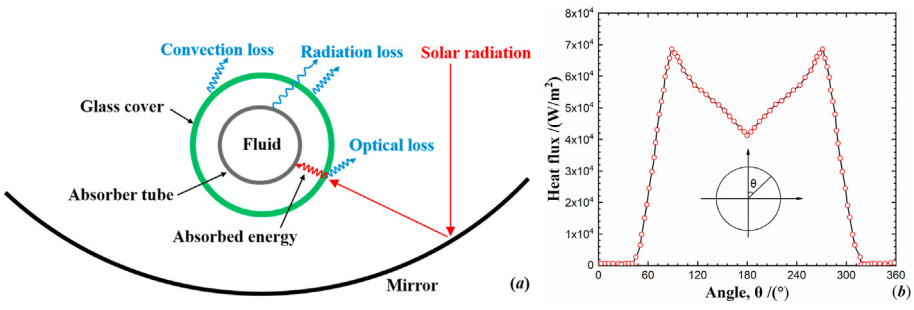

Fig. 1. (a) Parabolic trough collector and (b) absorber tube wall heat flux.

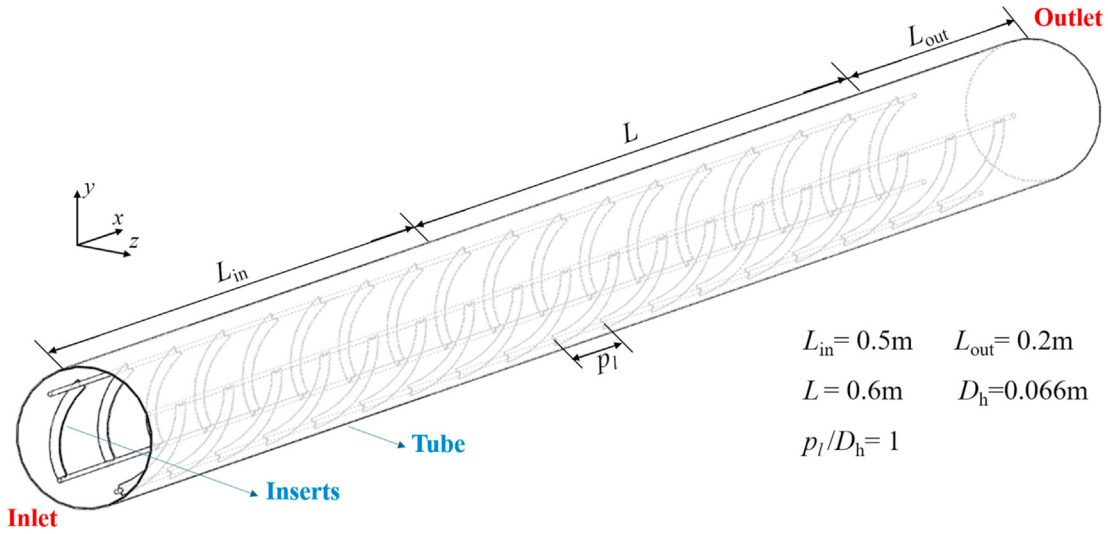

Fig. 2. The present research model.

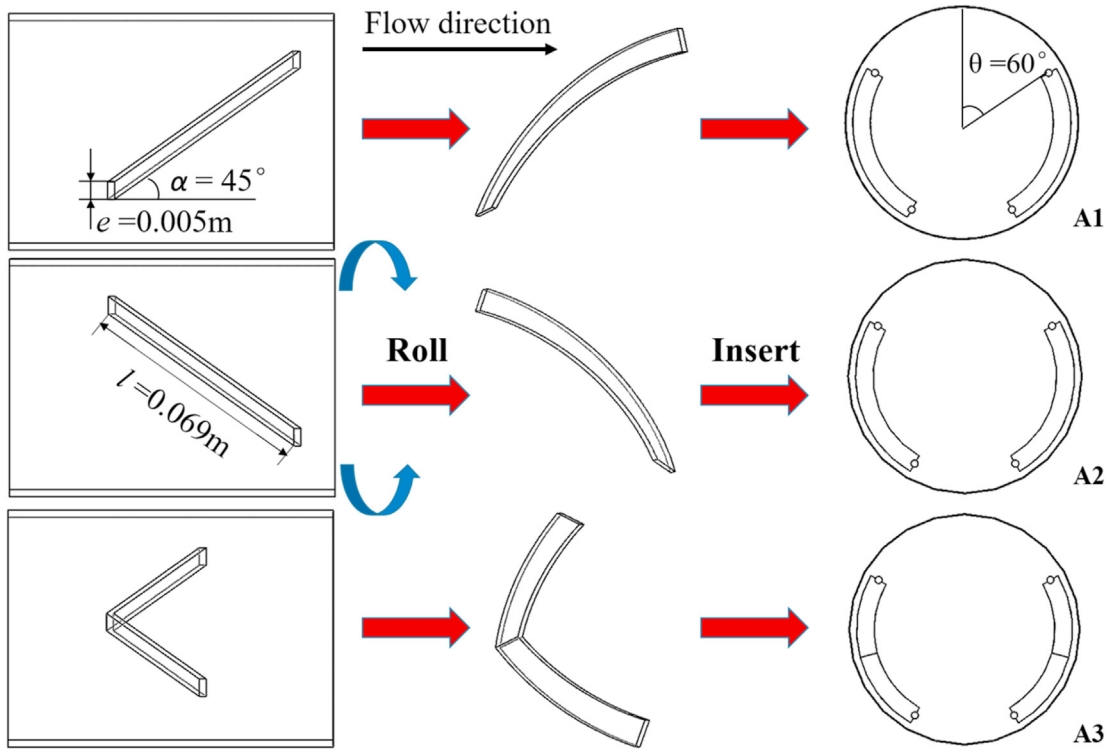

Fig. 3. Three types of curved-twisted baffles.

$\sigma_k = 1$, $\sigma_\varepsilon = 1.2$, $C_1 = \max\left[0.43, \frac{Sk/\varepsilon}{Sk/\varepsilon+5}\right]$, $S = \sqrt{2S_{ij}S_{ij}}$, $C_2 = 1.9$, G_k represents the generation of turbulence kinetic energy due to the mean velocity gradients. The relationship between dynamic viscosity (μ) and temperature is given as [15]:

$$\mu = 8.4866 \times 10^{-2} - 5.5412 \times 10^{-4}T + 1.3882 \times 10^{-6}T^2 - 1.5660 \times 10^{-9}T^3 + 6.6720 \times 10^{-13}T^4 \quad (6)$$

At different inlet temperature, the density, thermal conductivity, and specific thermal capacity are given in Table 1 [22].

Table 1
Thermal properties of Syltherm 800.

T/K	κ /W·m^{-1}·K^{-1}	ρ /kg·m^{-3}	c_p/J·kg^{-1}·K^{-1}
400	0.1149	840.3	1791
450	0.1055	794.8	1876
500	0.0961	747.2	1962
550	0.0867	696.2	2047
600	0.0773	640.0	2133

Table 2
The detail parameters in Fourier formulas of heat flux distribution.

θ_0	ω	a_0	a_1	b_1	a_2	b_2
$0° \le \theta_0 < 41.6°$	0	680	0	0	0	0
$41.6° \le \theta_0 < 88.6°$	0.0588	35,120	25,470	−24250	1464	−671
$88.6° \le \theta_0 \le 180°$	0.0312	56,160	−11290	10,510	−4039	−1582

3.2. Boundary conditions

At the inlet, velocity and temperature profiles are both uniform. The pressure outlet boundary condition is specified at the outlet. The absorber tube wall is no-slip for the velocity boundary. Besides, the inserts wall is no-slip for velocity and adiabatic for temperature. In addition, a non-uniform heat flux distribution shown in Fig. 1(*b*) is imposed on the absorber wall. In this paper, the non-uniform wall heat flux is assumed to be constant. The corresponding Fourier formulas given by Liu et al. [16] are expressed as

$$q = a_0 + a_1\cos(\omega\theta_0) + b_1\sin(\omega\theta_0) + a_2\cos(2\omega\theta_0) + b_2\sin(2\omega\theta_0) \quad (7)$$

where $\theta_0 = \theta$ for $0° \le \theta < 180°$, $\theta_0 = 360° - \theta$ for $180° \le \theta < 360°$, and the detail parameters in Fourier formulas are listed in Table 2.

3.3. Parameter definitions

The Reynolds number (Re) and convective heat transfer coefficient (h) are defined respectively as:

$$\mathrm{Re} = \frac{\rho u_\mathrm{m} D_\mathrm{h}}{\mu} \quad (8)$$

$$h = \frac{q}{T_\mathrm{r} - T_\mathrm{f}} \quad (9)$$

where u_m is the inlet mean velocity, q is the average heat flux on the absorber tube wall, T_r is absorber wall temperature, and T_f is the fluid bulk temperature.

The friction factor (f) and Nusselt number (Nu) are expressed respectively as:

$$f = \frac{\Delta p}{(L/D_\mathrm{h})\rho u_\mathrm{m}^2/2} \quad (10)$$

$$Nu = \frac{hD_\mathrm{h}}{\kappa} \quad (11)$$

where Δp is the pressure difference in the test section.

The wall temperature uniformity performance is characterized by the wall temperature difference given as T_{max}-T_{min} and T_{btm}-T_{tpm}. The parameters T_{max}, T_{min}, T_{btm}, and T_{tpm} are maximum wall temperature, minimum wall temperature, bottom half tube wall temperature, and top half tube wall temperature, respectively. The T_{max}-T_{min} is the maximum wall temperature difference. The T_{btm}-T_{tpm} is the mean wall temperature difference between the bottom half tube and the top half tube. Reducing T_{max}-T_{min} and T_{btm}-T_{tpm} is beneficial to preventing excessive high wall temperature and decreasing tube bending.

In order to evaluate the solar thermal conversion performance with considering the pump power consumption, the overall efficiency and exergy efficiency are adopted. The efficiencies are calculated mathematically through applying the enhanced heat transfer coefficient and friction factor to the practical heat transfer process.

Energy efficiency. The absorbed useful heat and heat loss can be expressed respectively as:

$$Q_\mathrm{u} = A_\mathrm{r} h\left(T_\mathrm{r} - T_\mathrm{f}\right) \quad (12)$$

$$Q_\mathrm{loss} = A_\mathrm{r} U_\mathrm{L}(T_\mathrm{r} - T_a) \quad (13)$$

where A_r is absorber wall area, U_L is heat loss coefficient, and the ambient temperature T_a is equal to 298.15 K.

The heat loss coefficient U_L can be obtained through analyzing the heat transfer process. Neglecting the heat loss through heat conduction, the heat loss is equal to the radiative heat transfer between the metallic tube and glass cover. It is expressed as:

$$Q_\mathrm{loss} = A_\mathrm{r}\sigma\left(T_\mathrm{r}^4 - T_\mathrm{c}^4\right) \Big/ \left(1/\varepsilon_\mathrm{r} + A_\mathrm{r}(1-\varepsilon_\mathrm{c})/(\varepsilon_\mathrm{c}A_\mathrm{c})\right) \quad (14)$$

where σ is Boltzmann constant that is equal to 5.67×10^{-8} W/(m^2·K^4), T_c and A_c are glass cover temperature and glass cover area respectively, ε_r and ε_c are metallic tube emissivity and glass cover emissivity respectively. In this paper, ε_c is 0.86 and ε_r is calculated with [22]:

$$\varepsilon_\mathrm{r} = 0.05599 + 1.039 \times 10^{-4} T_\mathrm{r} + 2.249 \times 10^{-7} T_\mathrm{r}^2 \quad (15)$$

The heat loss is also equal to the sum of radiative heat loss and convective heat loss from the glass cover. It is expressed as:

$$Q_\mathrm{loss} = A_\mathrm{c}\varepsilon_\mathrm{c}\sigma\left(T_\mathrm{c}^4 - T_\mathrm{sky}^4\right) + A_\mathrm{c}h_\mathrm{c}(T_\mathrm{c} - T_a) \quad (16)$$

where the convective heat transfer coefficient (h_c) is usually approximately 10 W/(m^2·K). The sky temperature (T_sky) is calculated with [22]:

$$T_\mathrm{sky} = 0.0552 T_a^{1.5} \quad (17)$$

In addition, the total irradiation solar energy from the sun is expressed as:

$$Q_\mathrm{s} = A_\mathrm{r} U_\mathrm{L}(T_\mathrm{r} - T_a) + A_\mathrm{r} h\left(T_\mathrm{r} - T_\mathrm{f}\right) \quad (18)$$

Thus, the Q_u can be obtained through simultaneously solving Eqs. (12)–(18) with given Q_s and h.

The thermal efficiency can be expressed as:

$$\eta_\mathrm{th} = Q_\mathrm{u}/Q_\mathrm{s} \quad (19)$$

with taking the pump power consumption (P_w) into consideration, the overall efficiency is written as:

$$\eta_\mathrm{ovr} = \left(Q_\mathrm{u} - P_\mathrm{w}/\eta_\mathrm{elc}\right)/Q_\mathrm{s} \quad (20)$$

where the electricity efficiency η_elc is given as 0.33 [4,8].

Exergy efficiency. The exergy input from the solar irradiation is equal to the sum of the absorbed useful exergy output and total exergy destruction. The exergy balance equation can be written as:

$$(1 - T_a/T_\mathrm{s})Q_\mathrm{s} = m(\Delta h - T_a\Delta s) + E_\mathrm{xd} \quad (21)$$

According to Petala model [4], the apparent sun temperature (T_s) is approximately 4500 K [29]. For liquids, the enthalpy difference (Δh) and entropy difference (Δs) are expressed respectively as:

$$\Delta h = h_{out} - h_{in} = c_p\left(T_{f,out} - T_{f,in}\right) \tag{22}$$

$$\Delta s = s_{out} - s_{in} = c_p \ln\frac{T_{f,out}}{T_{f,in}} - \frac{p_{out} - p_{in}}{\rho T_f} \tag{23}$$

Thus, the exergy efficiency is expressed as:

$$\eta_{ex} = 1 - \frac{E_{xd}}{(1 - T_a/T_s)Q_s} \tag{24}$$

3.4. Computational methods

The computational results are obtained with commercial software FLUENT 16.0. The computational domain is covered by an unstructured mesh which is generated with commercial software ICEM 16.0. The governing equations are discretized by using finite volume method with second order scheme for pressure and second order upwind scheme for other quantities. The SIMPLE algorithm [30–32] is applied to handle the coupling of velocity and pressure. The enhanced wall function is activated in the turbulence model. When the relative residuals are decreased to 10^{-3} for continuity equation, 10^{-8} for energy equation, and 10^{-5} for other equations, or all quantities change little, the calculation can be considered converged.

3.5. Results verifications

The grid independence verification is shown in Fig. 4. At the mass flux rate of 5.67 kg/s with inserting A1 type ICTBs, the Nusselt number and friction factor vary with the increase of grid number. As the grid number increases from 7.65 million to 12.02 million, the variations of Nusselt number and friction factor are 0.32% and 1.13%, respectively. It means that the grid system with total grid number of 7.65 million is dense enough. Thus, this paper selects the grid system of 7.65 million grid number. Besides, the selected grid system details are also shown in Fig. 4. The mesh is extremely dense near the absorber wall so as to guarantee $y^+ < 1$. In the core flow region, hexahedral mesh is generated to capture the flow characteristics. In addition, due to the similarity among A1, A2, and A3, this grid system is used to get reliable results in the following work.

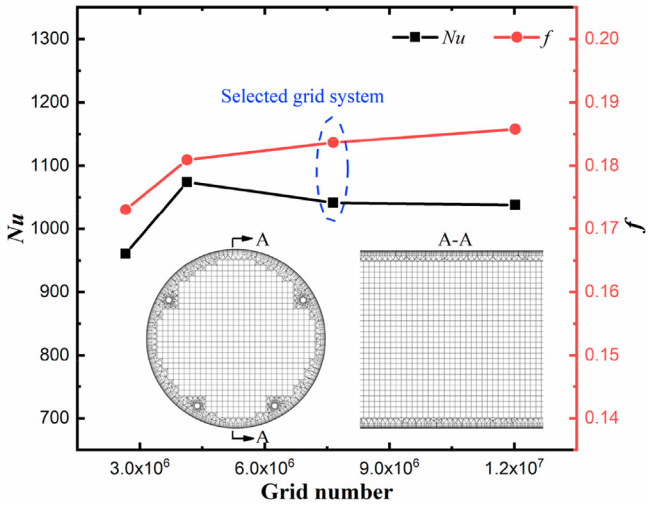

Fig. 4. Grid independence verification.

The results are dependent on the selection of test section. In the practical parabolic trough collector, the absorber tube is long enough so that most region of the tube is not affected by the inlet and outlet effects in terms of thermal hydraulic performance. Thus, it is necessary to find a test section which is not affected by the inlet and outlet effects. Fig. 5 shows the variations of local Nusselt number and friction factor along the flow direction at the mass flux rate of 1.13 kg/s with inserting different types of ICTBs. It shows that the results are periodic in the present test section. The results from the test section are not affected by the inlet and outlet effects. Thus, the selection of test section is reliable.

As depicted in Fig. 6, the present results are compared with the empirical correlations and experimental results in the literature for results verification. The Gnielinski correlation for Nusselt number and Petukhov correlation for friction factor are expressed respectively as [33]:

$$Nu_0 = \frac{(f/8)(\mathrm{Re} - 1000)\mathrm{Pr}}{1 + 12.7(f/8)^{0.5}\left(\mathrm{Pr}^{2/3} - 1\right)} \tag{25}$$

$$f_0 = (1.82\lg\mathrm{Re} - 1.64)^{-2} \tag{26}$$

The multiplier $(\mathrm{Pr}/\mathrm{Pr_w})^c$ is used for correction due to variations of properties, where c is 0.11 for Nusselt number and −0.25 for friction factor [34]. As depicted in Fig. 6(a), the maximum deviations of Nusselt number and friction factor between present results and correlations are 8.3% and 8.4%, respectively. It shows good agreements between the present results and the empirical correlations with the increase of mass flow rate.

In Fig. 6(*b*), the present calculated thermal efficiency is compared with the experimental results [24]. The experimental results are also chosen for verification in other works [12,16,22]. In this paper, the present thermal efficiency is calculated with Eq. (19) by using the present convective heat transfer coefficient. The deviation between the calculated thermal efficiency and the experimental thermal efficiency is less than 1.58% with inlet temperature increasing from 375 K to 630 K. It shows that the present method for obtaining thermal efficiency is reliable.

The above results verifications indicate that the present obtained results are reliable and accurate enough.

4. Results and discussions

In the following context, this paper will investigate the effect of longitudinal swirls impinging cooling method (SICM) on reducing wall temperature by inserting three types of inclined curved-twisted baffles (ICTB) in the PTC. Besides, the performance comparisons will be carried out with the variations of mass flow rate and inlet temperature.

4.1. Performance enhancement mechanism

4.1.1. Flow characteristics

Fig. 7 shows the streamlines in the enhanced PTC at mass flow rate of 1.13 kg/s and inlet temperature of 400 K. The streamlines are bent due to the fluid deflection caused by baffles. Compared with A3 type, the A1 type and A2 type generate more curved streamlines. In the front view, each of the A1 type and A2 type generates a pair of swirls while the A3 type generates two pairs of swirls. Thus, the multi-longitudinal swirls flow is generated by inserting ICTBs in the PTC.

Fig. 8 shows the tangential velocity distributions at the cross section of $x = 0.8$ m. With the formation of longitudinal swirls flow, cold fluids flow from the core region to the boundary region,

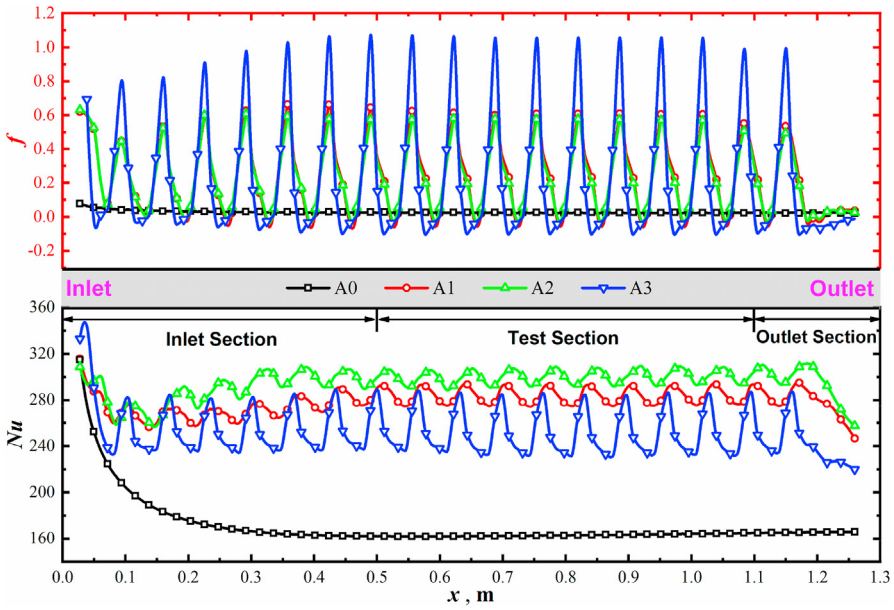

Fig. 5. Test section verification: local *Nu* and *f* along the flow direction.

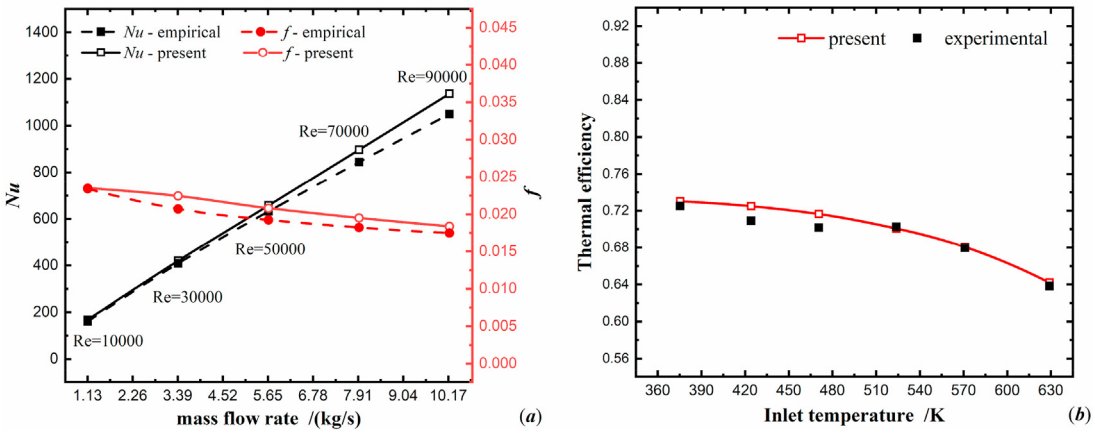

Fig. 6. Results verification: (*a*) mass flow rate variations, (*b*) inlet temperature variations.

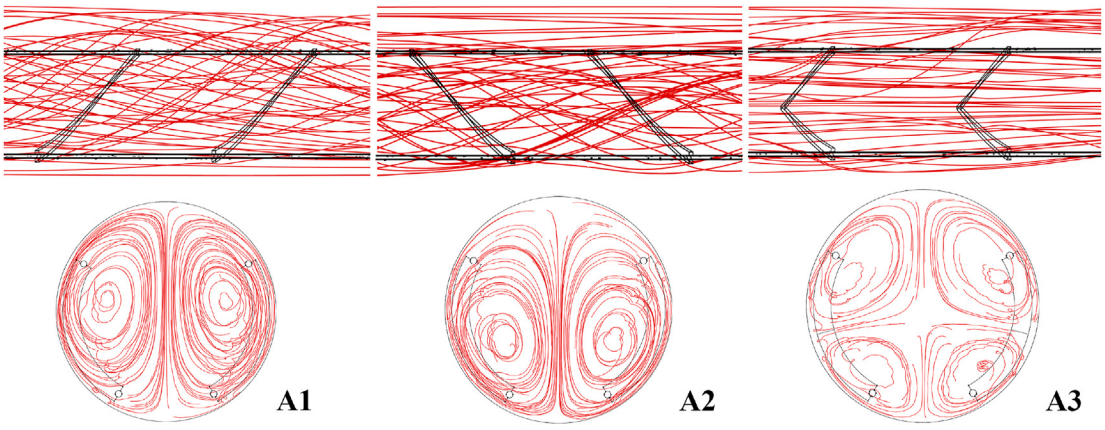

Fig. 7. Streamlines comparisons among three types of ICTBs.

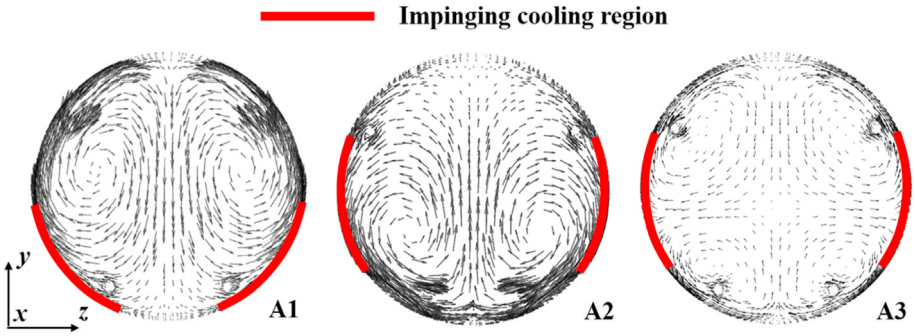

Fig. 8. Tangential velocity distributions at the cross section of $x = 0.8$ m.

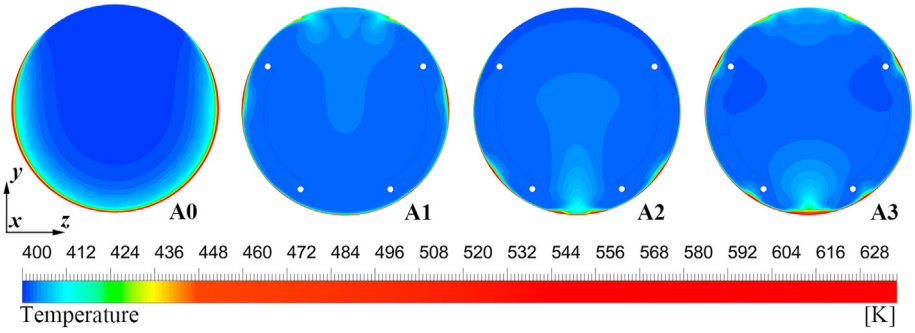

Fig. 9. Temperature distributions at the cross section of $x = 0.8$ m.

thereby impinging the absorber wall. The cold fluid impinging is conducive to wall temperature reduction. The impinged regions on the wall are denoted by red lines. As depicted in Fig. 8, the impinging cooling region of A1 type is on the bottom half of the tube wall where the heat flux is extremely high. It means that the A1 type is exactly for reducing the local high wall temperature in the PTC. In order to display the wall temperature cooling effect, Fig. 9 shows the comparison of temperature distributions at the

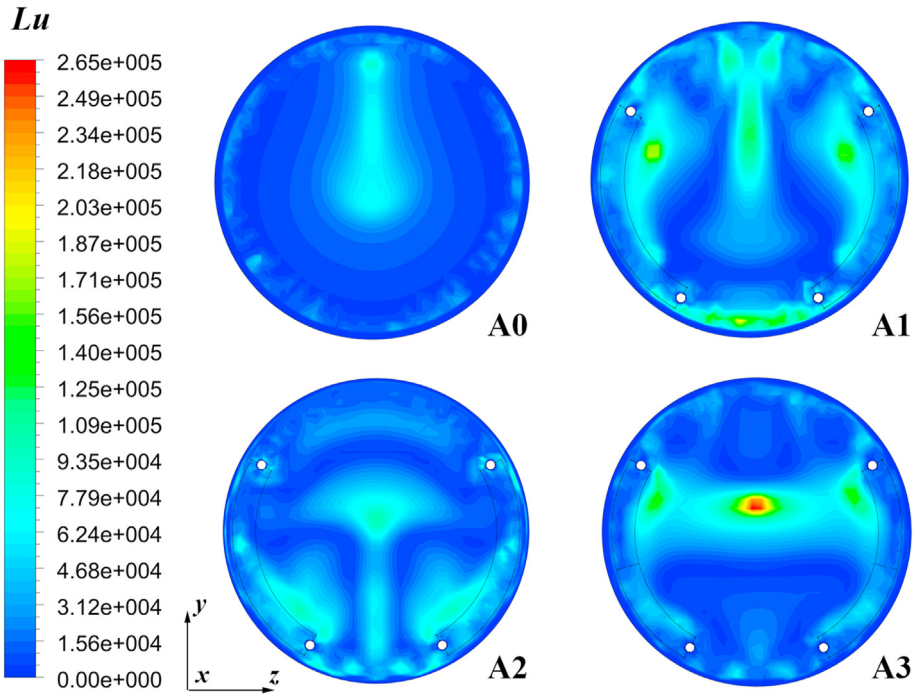

Fig. 10. The comparison of *Lu* distributions at the cross section of $x = 0.8$ m.

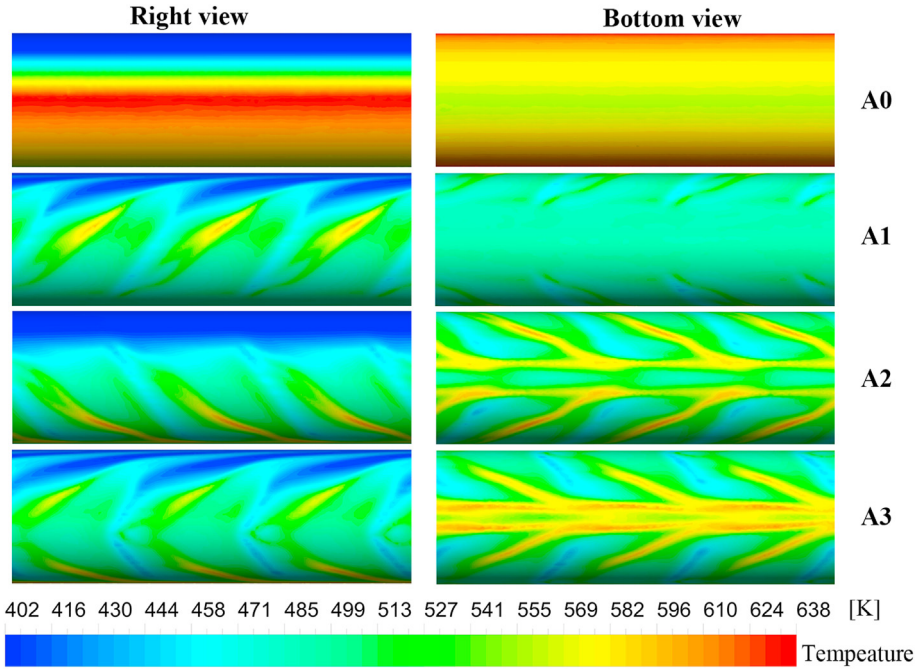

Fig. 11. Comparisons of wall temperature distributions at 0.5 m < x < 0.7 m.

cross section of $x = 0.8$ m. Compared with the plain absorber tube (A0), the thermal boundary layer is thinned in enhanced absorber tubes with three kinds of ICTBs (A1, A2, and A3). Owing to the impinging effect, the high temperature region on the enhanced absorber tube wall is reduced significantly. It indicates that the convective heat transfer is enhanced. In particular, the high temperature region of bottom half tube wall in the A1 type is less than that in A2 and A3 types. It indicates that the A1 type is more effective in reducing the high temperature on the bottom half tube wall of PTC.

4.1.2. Heat convection performance

Heat convection velocity [35,36] is the component of fluid velocity in temperature gradient direction. Its magnitude is expressed as

$$V_h = \frac{\mathbf{U}\cdot\nabla T}{|\nabla T|} = |\mathbf{U}|\cos\beta \tag{27}$$

where β is the included angle between velocity and temperature gradient.

The term $\rho c_p V_h$ can be used to represent the local heat convection intensity. In order to describe the local heat convection performance efficiently, the Lu number is introduced as

$$Lu = \frac{\rho c_p |V_h| D_h}{\kappa} \tag{28}$$

In this way, the local heat convection intensity can be visualized by displaying the contours of Lu. In order to reducing local high wall temperature, it is necessary to increase the Lu near the bottom half wall.

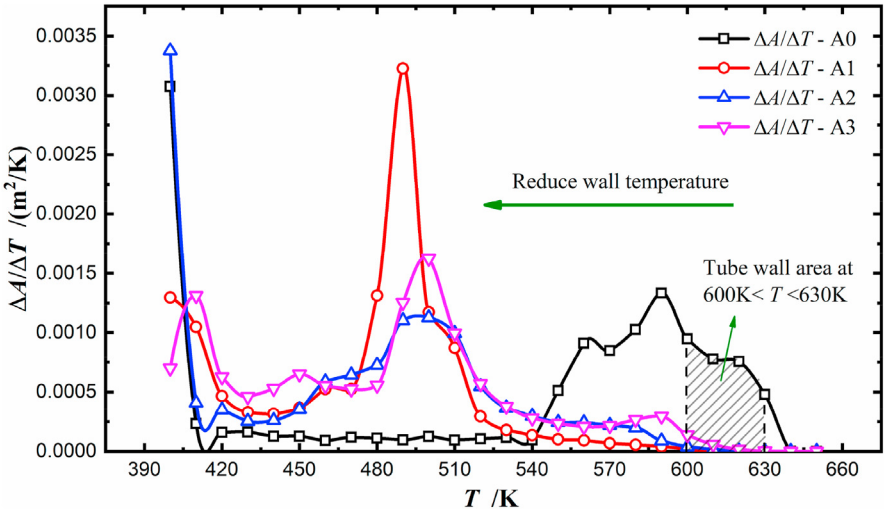

Fig. 12. Tube wall area distributions at different wall temperature.

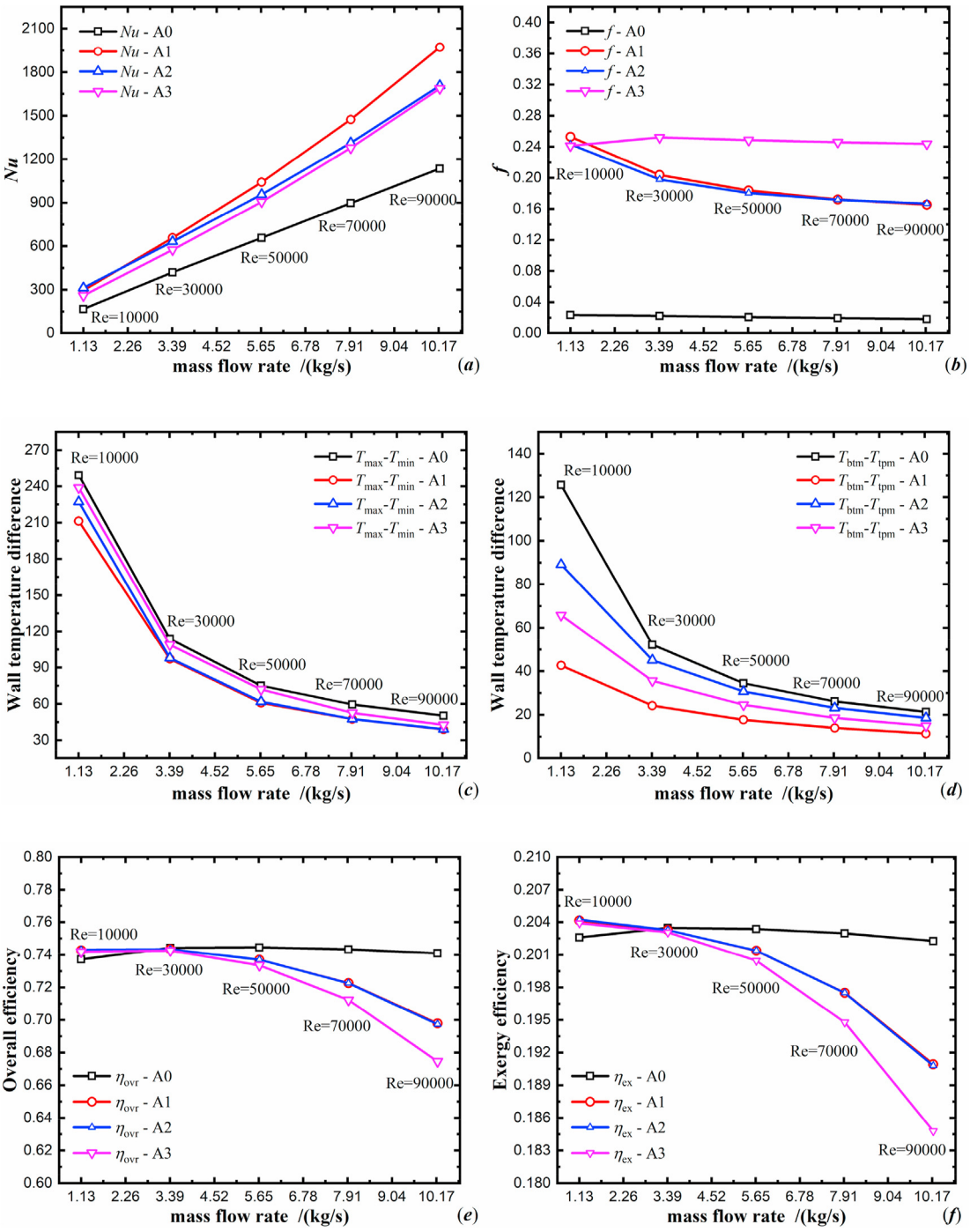

Fig. 13. Variations of (*a*) *Nu*, (*b*) *f*, (*c*) T_{max}-T_{min}, (*d*) T_{btm}-T_{tpm}, (*e*) η_{ovr}, (*f*) η_{ex} with the increase of mass flow rate.

Fig. 10 shows the *Lu* distributions at the cross section of $x = 0.8$ m. The mass flow rate is 1.13 kg/s and inlet temperature is 400 K. The A0 type represents the plain tube without heat transfer enhancement components. With inserting different ICTBs in the absorber tube, the velocity distributions are changed greatly, which also leads to the changes in synergy angle β. Thus, there are great changes in *Lu* distributions. Near the bottom half wall, the *Lu* is increased in most region. It means that the local heat convection performance is increased near the high temperature wall. Especially, the A1 type generates larger *Lu* near the bottom wall compared with A2 and A3 types.

4.1.3. Wall temperature distribution

The wall temperature distributions comparisons are shown in Fig. 11 at mass flow rate of 1.13 kg/s and inlet temperature of 400 K. The wall temperature distributions are changed greatly in three enhanced tubes compared with that in the plain tube. In the right view, the high wall temperature area is always reduced significantly with inserting different types of ICTBs. It means that the A1, A2, and A3 are all effective in wall temperature reduction by applying longitudinal swirls impinging cooling method. In A1 and A3 types, the warmer fluid near the bottom half wall is deflected to the top half wall, thereby generating some slightly higher

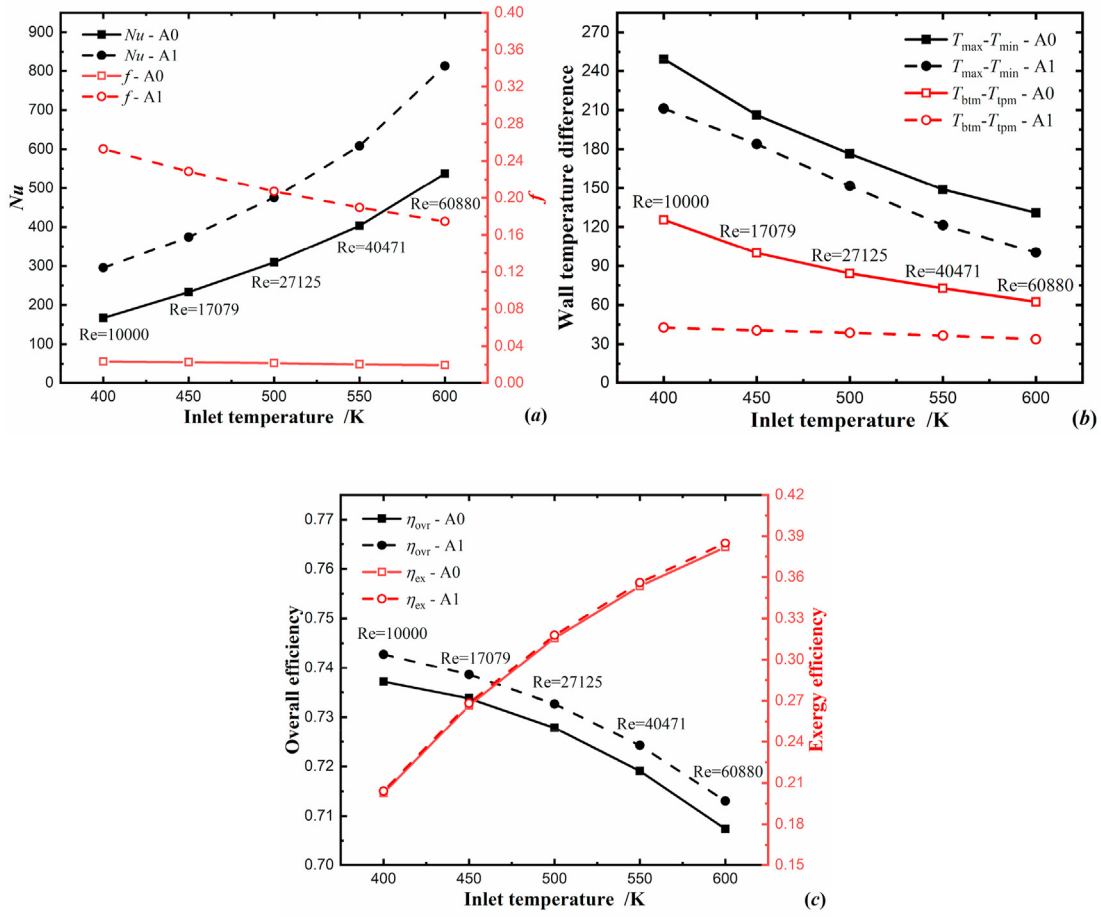

Fig. 14. Variations of (*a*) *Nu* and *f*, (*b*) wall temperature difference, (*c*) η_{ovr} and η_{ex} with the increase of inlet temperature.

temperature region in the top half wall compared with that in the plain type tube. In the bottom view, the bottom wall temperature is reduced significantly in A1 type. In A2 and A3 types, the wall temperature is still high in some bottom region due to the low local heat convection performance caused by fluid hedging between the rear edges of ICTBs. Generally, the wall temperature near the upwind side of the ICTB is lower than that near the downwind side of the ICTB. It is due to the thermal boundary thinning caused by the flow deflection in the upwind side of the ICTB. Besides, the wall temperature near the front edge of ICTB is lower than that near the rear edge of ICTB. It owes to the higher local heat convection near the front edge where the impinging cooling always appears. As a comparison result, it is better to arrange the front edge of ICTB in higher heat flux region.

In order to describe the wall temperature distribution quantitatively, Fig. 12 shows comparisons of the tube wall area distributions at different wall temperature. The mass flow rate is 1.13 kg/s and the inlet temperature is 400 K. The total area between the curve and bottom axis is the total area of the absorber tube wall. As is shown, the tube wall area is broad when the wall temperature is beyond 540 K in the plain tube. With inserting the ICTBs in the PTC, the tube wall area with temperature beyond 540 K is reduced significantly. The wall temperature reduction is conducive to guaranteeing the performance of selective coating. As a comparison result, the A1 type is the best in reducing high wall temperature.

4.2. Mass flow rate variations

Fig. 13 shows the performance comparisons among the plain tube (A0) and three enhanced tubes (A1, A2, and A3) with the increase of mass flow rate at the inlet temperature of 400 K. As depicted in Fig. 13(*a*) and (*b*), the variation ranges of Nu/Nu_0 and f/f_0 are 1.41–1.95 and 9.39–13.95, respectively. The enhanced heat transfer performance of the A1 type is more than that of A2 and A3 types in most cases. The reason is that the A1 type can reduce the bottom half tube wall temperature more effectively, thereby reducing the average temperature of the tube wall. When the mass flow rate is 1.13 kg/s, the top half tube wall temperature of A2 type is much lower than others, which leads to a larger *Nu*. The friction factor of A3 type is more than that of A1 and A2 types in most cases. It is due to the generated two pairs of vortices in the A3 type tube, which increases the viscous dissipation. When the mass flow rate is 1.13 kg/s, the fluid viscosity near the wall of A3 type tube is much smaller due to the higher wall temperature, thereby leading to the reduction in friction factor.

In Fig. 13(*c*) and (*d*), T_{max}, T_{min}, T_{btm}, and T_{tpm} are maximum wall temperature, minimum wall temperature, bottom half tube wall temperature, and top half tube wall temperature, respectively. The decrease of T_{max}-T_{min} is benefit to preventing local high wall temperature. The decrease of T_{btm}-T_{tpm} is benefit to preventing tube bending. As is shown, the T_{max}-T_{min} and T_{btm}-T_{tpm} are both decreased with the increase of mass flow rate. It is owing to the increased convective heat transfer performance as the mass flow

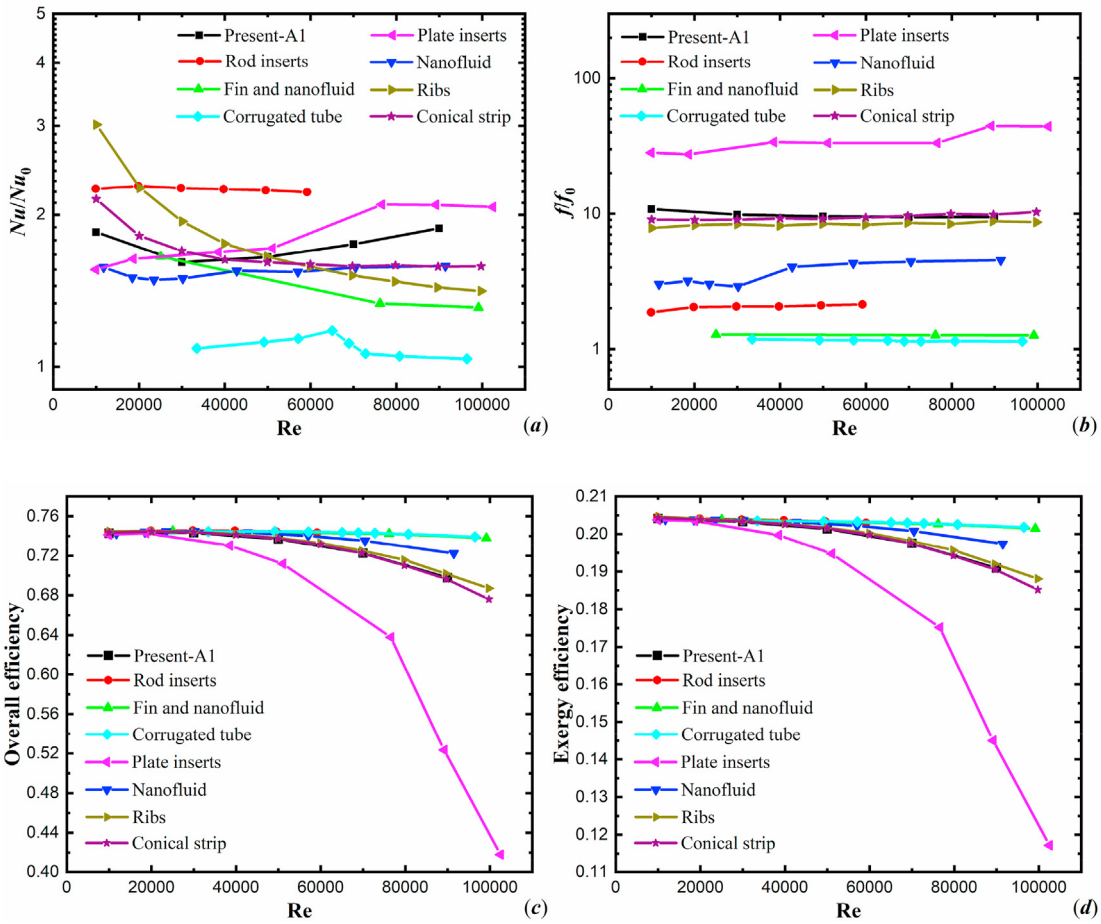

Fig. 15. Comparisons between present work and literatures: (*a*) Nu/Nu_0, (*b*) f/f_0, (*c*) η_{ovr}, and (*d*) η_{ex}.

rate increases. Thus, it is more necessary to take heat transfer enhancement measures to uniform the wall temperature at low mass flow rate. Besides, the A1 type is the best in wall temperature uniformity performance among three enhanced tubes. As the mass flow rate increases in A1 type tube, the maximum wall temperature difference is decreased by 14.7%–22.6% while the mean temperature difference between top half wall and the bottom half wall is decreased by 46.6%–66.0%.

Fig. 13(*e*) and (*f*) show the overall efficiency comparisons and exergy efficiency comparisons, respectively. The overall efficiency and exergy efficiency in the enhanced tubes are larger than those in the plain tube when the mass flow rate is less than 3.4 kg/s. When the mass flow rate is greater than 3.4 kg/s, the convective heat transfer performance is high due to the increase of Reynolds number, leading to small heat loss in the plain tube. In this way, the use of heat transfer enhancement measures harvests small increase in absorbed energy which cannot exceed the heat loss amount in the plain tube. However, the increase of mass flow rate leads to much pump power consumption. Thus, the overall efficiency and exergy efficiency are both decreased. In order to guarantee the operation safety, it deserves the sacrifice in efficiencies. Furthermore, the overall efficiency and exergy efficiency in A1 type tube are almost the same as those in the A2 type tube and overwhelm those in the A3 type tube.

Through the investigations on flow characteristics, temperature distributions, and mass flow variations, the A1 type is considered as the best type. Thus, the A1 type is chosen to study the effect of inlet temperature variation on thermal hydraulic performance and wall temperature difference at the mass flow rate of 1.13 kg/s in the following context.

4.3. Inlet temperature variations

A practical solar thermal collector system is consisted of several thermal collector units in series [4]. The temperature of the working fluid is varied from low level to high level in a whole thermal collection process. Hence, it is significant to investigate the performance at the working temperature from low level to high level in the PTC. It shows in Fig. 14 the comparisons of *Nu*, *f*, wall temperature difference, η_{ovr}, and η_{ex} between A0 type and A1 type with the increase of inlet temperature at the mass flow rate of 1.13 kg/s. Compared with the plain A0 type tube, the variations of Nu/Nu_0 and f/f_0 are 1.64–1.85 and 9.71–10.80 in the A1 type tube, respectively. Besides, the maximum wall temperature difference is decreased by 10.8%–23.4% with an average value of 16.4% in the A1 type tube. The mean temperature difference between the bottom half wall and the top half wall is decreased by 46.1%–66.0% with an average value of 55.1% in the A1 type tube. It means that the A1 type is always excellent in the aspect of preventing tube bending. In addition, with the increase of inlet temperature, the overall efficiency and exergy efficiency are always increased in the A1 type tube at the mass flow rate of 1.13 kg/s. The overall efficiency is increased by 0.48%–0.56% with an average value of 0.52%. The exergy efficiency is increased by 0.15%–0.31% with an average value of 0.22%. It means that the pump power consumption is moderate so that the efficiencies are increased. It is worth noting that the core

purpose of this paper is to decrease the wall temperature and reduce tube bending. The above results indicate that this purpose has been achieved with inserting A1 type ICTBs in the PTC.

4.4. Comparisons

In this work, the inclined curved twisted baffles successfully reduce the local high wall temperature, thereby improving the tube wall temperature uniformity. It demonstrates the effectiveness of longitudinal swirls impinging cooling method. As it is known, the energy and exergy efficiencies are also important for the PTC. Thus, in order to objectively display the achieved performance, this paper provides comparisons of Nu/Nu_0, f/f_0, η_{ovr}, and η_{ex} between the present work and literatures with the variation of Reynolds number, as depicted in Fig. 15.

The present A1 type with the inlet temperature of 400 K is chosen for comparison. The previous typical works are rod inserts [37], tube fins combined nanofluids [38], corrugated tube [39], plate inserts [14], nanofluids [40], tube ribs [12], and conical strip inserts [16]. As for the data from literatures, the Nu/Nu_0 and f/f_0 are taken from literatures directly. Considering the differences in different literatures, such as working fluids, selective coating, operation temperature, parabolic trough collector parameters, and et al., this paper mathematically recalculates the overall efficiency and exergy efficiency for effective comparisons by applying the Nu/Nu_0 and f/f_0 from the literature to the present operation conditions. As shown in Fig. 15, the absorber tube with the ICTBs has moderate enhancement in Nu and f compared with other works. Besides, the energy and exergy efficiencies are also moderate among those works. Moreover, it is worth noting that the present ICTBs are prominent in improving the wall temperature uniformity.

5. Conclusions

In this paper, three types of novel ICTBs were devised to decrease and uniform the wall temperature of absorber tube with moderate pump power consumption in the PTC. Typical conclusions were drawn as follows:

(a) The longitudinal swirls impinging cooling method was effective in reducing the local high wall temperature. As the longitudinal swirls flow was generated, some cold fluids flowed from the core region to the boundary region, thereby impinging the absorber wall. The impinging cooling always appeared near the front edge of ICTBs. It was suggested to arrange the front edge of ICTB in higher heat flux region.

(b) The A1 and A2 types each generated a pair of longitudinal swirls while the A3 type generated two pairs of longitudinal swirls. The A1, A2, and A3 types were all effective in wall temperature reduction. The impinging cooling region of A1 type was exactly on the bottom half tube where the local wall temperature was high. The A1 type was the best in wall temperature uniformity performance among three baffles.

(c) When the mass flow rate is less than 3.4 kg/s, the overall efficiency and exergy efficiency in the enhanced tubes were larger than those in the plain tube. Besides, the efficiencies in A1 type tube were almost the same as those in the A2 type tube and overwhelmed those in the A3 type tube.

(d) As the inlet temperature increased from 400 K to 600 K at a mass flow rate of 1.13 kg/s in the A1 type tube, the variations of Nu/Nu_0 and f/f_0 are 1.64–1.85 and 9.71–10.80, respectively. Besides, the average T_{max}-T_{min} and T_{btm}-T_{tpm} were decreased by 16.4% and 55.1%, respectively. In addition, the average overall efficiency and exergy efficiency were increased by 0.52% and 0.22%, respectively.

CRediT authorship contribution statement

Hui Xiao: Conceptualization, Methodology, Validation, Formal analysis, Investigation, Data curation, Writing - original draft. **Peng Liu:** Methodology, Validation, Formal analysis. **Zhichun Liu:** Resources, Supervision, Project administration. **Wei Liu:** Resources, Supervision, Project administration, Funding acquisition.

Declaration of competing interest

The authors declare that they have no known competing financial interests or personal relationships that could have appeared to influence the work reported in this paper.

Acknowledgement

This work was supported by the National Natural Science Foundation of China (Grant No. 51736004).

References

[1] F. Wang, Z. Cheng, J. Tan, Y. Yuan, Y. Shuai, L. Liu, Progress in concentrated solar power technology with parabolic trough collector system: a comprehensive review, Renew. Sustain. Energy Rev. 79 (2017) 1314–1328.
[2] İ.H. Yılmaz, A. Mwesigye, Modeling, simulation and performance analysis of parabolic trough solar collectors: a comprehensive review, Appl. Energy 225 (2018) 135–174.
[3] Y.-L. He, Y. Qiu, K. Wang, F. Yuan, W.-Q. Wang, M.-J. Li, J.-Q. Guo, Perspective of concentrating solar power, Energy 198 (2020) 117373.
[4] E. Bellos, C. Tzivanidis, Alternative designs of parabolic trough solar collectors, Prog. Energy Combust. Sci. 71 (2019) 81–117.
[5] N.u. Rehman, M. Uzair, M. Asif, Evaluating the solar flux distribution uniformity factor for parabolic trough collectors, Renew. Energy 157 (2020) 888–896.
[6] E. Bellos, C. Tzivanidis, D. Tsimpoukis, Enhancing the performance of parabolic trough collectors using nanofluids and turbulators, Renew. Sustain. Energy Rev. 91 (2018) 358–375.
[7] J. Subramani, P.K. Nagarajan, O. Mahian, R. Sathyamurthy, Efficiency and heat transfer improvements in a parabolic trough solar collector using TiO2 nanofluids under turbulent flow regime, Renew. Energy 119 (2018) 19–31.
[8] A. Mwesigye, Z. Huan, J.P. Meyer, Thermal performance and entropy generation analysis of a high concentration ratio parabolic trough solar collector with Cu-Therminol®VP-1 nanofluid, Energy Convers. Manag. 120 (2016) 449–465.
[9] Y. Wang, J. Xu, Q. Liu, Y. Chen, H. Liu, Performance analysis of a parabolic trough solar collector using Al2O3/synthetic oil nanofluid, Appl. Therm. Eng. 107 (2016) 469–478.
[10] S. Akbarzadeh, M.S. Valipour, Energy and exergy analysis of a parabolic trough collector using helically corrugated absorber tube, Renew. Energy 155 (2020) 735–747.
[11] E. Bellos, C. Tzivanidis, Enhancing the performance of a parabolic trough collector with combined thermal and optical techniques, Appl. Therm. Eng. 164 (2020) 114496.
[12] P. Liu, J. Lv, F. Shan, Z. Liu, W. Liu, Effects of rib arrangements on the performance of a parabolic trough receiver with ribbed absorber tube, Appl. Therm. Eng. 156 (2019) 1–13.
[13] O.A. Jaramillo, M. Borunda, K.M. Velazquez-Lucho, M. Robles, Parabolic trough solar collector for low enthalpy processes: an analysis of the efficiency enhancement by using twisted tape inserts, Renew. Energy 93 (2016) 125–141.
[14] A. Mwesigye, T. Bello-Ochende, J.P. Meyer, Heat transfer and thermodynamic performance of a parabolic trough receiver with centrally placed perforated plate inserts, Appl. Energy 136 (2014) 989–1003.
[15] X. Zhu, L. Zhu, J. Zhao, Wavy-tape insert designed for managing highly concentrated solar energy on absorber tube of parabolic trough receiver, Energy 141 (2017) 1146–1155.
[16] P. Liu, N. Zheng, Z. Liu, W. Liu, Thermal-hydraulic performance and entropy generation analysis of a parabolic trough receiver with conical strip inserts, Energy Convers. Manag. 179 (2019) 30–45.
[17] W. Liu, P. Liu, J.B. Wang, N.B. Zheng, Z.C. Liu, Exergy destruction minimization: a principle to convective heat transfer enhancement, Int. J. Heat Mass Tran. 122 (2018) 11–21.
[18] H. Xiao, J. Wang, Z. Liu, W. Liu, Turbulent heat transfer optimization for solar air heater with variation method based on exergy destruction minimization principle, Int. J. Heat Mass Tran. 136 (2019) 1096–1105.
[19] N. Zheng, F. Yan, K. Zhang, T. Zhou, Z. Sun, A review on single-phase convective heat transfer enhancement based on multi-longitudinal vortices in heat exchanger tubes, Appl. Therm. Eng. 164 (2020) 114475.
[20] A. Mwesigye, T. Bello-Ochende, J.P. Meyer, Minimum entropy generation due

to heat transfer and fluid friction in a parabolic trough receiver with non-uniform heat flux at different rim angles and concentration ratios, Energy 73 (2014) 606–617.
[21] X. Song, G. Dong, F. Gao, X. Diao, L. Zheng, F. Zhou, A numerical study of parabolic trough receiver with nonuniform heat flux and helical screw-tape inserts, Energy 77 (2014) 771–782.
[22] E. Bellos, C. Tzivanidis, Investigation of a star flow insert in a parabolic trough solar collector, Appl. Energy 224 (2018) 86–102.
[23] Y.-L. He, K. Wang, Y. Qiu, B.-C. Du, Q. Liang, S. Du, Review of the solar flux distribution in concentrated solar power: non-uniform features, challenges, and solutions, Appl. Therm. Eng. 149 (2019) 448–474.
[24] V. Dudley, G. Kolb, M. Sloan, D. Kearney, SEGS LS2 Solar Collector-Test Results, Report of Sandia National Laboratories, USA, 1994. SANDIA94-1884.
[25] M.V. Bozorg, M. Hossein Doranehgard, K. Hong, Q. Xiong, CFD study of heat transfer and fluid flow in a parabolic trough solar receiver with internal annular porous structure and synthetic oil–Al2O3 nanofluid, Renew. Energy 145 (2020) 2598–2614.
[26] Y. Qiu, M.-J. Li, Y.-L. He, W.-Q. Tao, Thermal performance analysis of a parabolic trough solar collector using supercritical CO2 as heat transfer fluid under non-uniform solar flux, Appl. Therm. Eng. 115 (2017) 1255–1265.
[27] W.Q. Tao, Numerical Heat Transfer, second ed., Xi'an Jiaotong University Press, Xi'an, 2001.
[28] T.-H. Shih, W.W. Liou, A. Shabbir, Z. Yang, J. Zhu, A new k-ε eddy viscosity model for high Reynolds number turbulent flows, Comput. Fluids 24 (3) (1995) 227–238.
[29] H. Xiao, Z. Dong, Z. Liu, W. Liu, Heat transfer performance and flow characteristics of solar air heaters with inclined trapezoidal vortex generators, Appl. Therm. Eng. 179 (2020) 115484.
[30] S.V. Patankar, Numerical HeatTransfer and Fluid Flow, Hemisphere, Washington D.C., 1980.
[31] L.M.F. Moukalled, M. Darwish, The Finite Volume Method in Computational Fluid Dynamics, 2016.
[32] H. Xiao, J. Wang, Z. Liu, W. Liu, A consistent SIMPLE algorithm with extra explicit prediction — SIMPLEPC, Int. J. Heat Mass Tran. 120 (2018) 1255–1265.
[33] T.L. Bergman, A. Lavine, F.P. Incropera, D.P. Dewitt, Fundamentals of Heat and Mass Transfer, John Wiley & Sons New York, 2017.
[34] S. Kandlikar, S. Garimella, D. Li, S. Colin, M.R. King, Heat Transfer and Fluid Flow in Minichannels and Microchannels, second ed., elsevier, 2014.
[35] H. Xiao, Z. Dong, R. Long, K. Yang, F. Yuan, A study on the mechanism of convective heat transfer enhancement based on heat convection velocity analysis, Energies 12 (21) (2019) 4175.
[36] H. Xiao, Z. Liu, W. Liu, Conjugate heat transfer enhancement in the mini-channel heat sink by realizing the optimized flow pattern, Appl. Therm. Eng. 182 (2021) 116131.
[37] C. Chang, A. Sciacovelli, Z. Wu, X. Li, Y. Li, M. Zhao, J. Deng, Z. Wang, Y. Ding, Enhanced heat transfer in a parabolic trough solar receiver by inserting rods and using molten salt as heat transfer fluid, Appl. Energy 220 (2018) 337–350.
[38] B. Amina, A. Miloud, L. Samir, B. Abdelylah, J.P. Solano, Heat transfer enhancement in a parabolic trough solar receiver using longitudinal fins and nanofluids, J. Therm. Sci. 25 (5) (2016) 410–417.
[39] W. Fuqiang, T. Zhexiang, G. Xiangtao, T. Jianyu, H. Huaizhi, L. Bingxi, Heat transfer performance enhancement and thermal strain restrain of tube receiver for parabolic trough solar collector by using asymmetric outward convex corrugated tube, Energy 114 (2016) 275–292.
[40] A. Mwesigye, Z. Huan, J.P. Meyer, Thermodynamic optimisation of the performance of a parabolic trough receiver using synthetic oil–Al2O3 nanofluid, Appl. Energy 156 (2015) 398–412.